ENGINEER - Vol. LIX, No. 02, pp. [145- 152], 2026

DOI: https://doi.org/10.4038/engineer.v59i2.7755

Variation of Fatigue Threshold Limit of Ti-6Al-4Vat Different Stress Ratios

Ruminda J. Wimalasiri

Abstract: Numerous factors affect the propensity of a metal to fatigue, especially the surface heterogeneities and the surface stress (residual stress) states. S-N curves are generally developed using smooth-polished specimens which give the fatigue limit of the microstructural short crack state. However, the threshold curves (Kitagawa-Takahashi type diagrams) provide a clear insight of the fatigue threshold conditions. These threshold curves correlate the S-N properties and fracture mechanics-based damage tolerant approach to understand the safe fatigue envelop of the materials. Specifically, according to the stress amplitude and surface damage (roughness), the fatigue threshold limits can be investigated. Rotary-bending tests were conducted using samples with four known surface roughness values (0.2 µm, 6 µm, 21 µm and 52 µm) with two subsets, annealed and without-annealed conditions. Residual stress states were examined, and they vary between -313 MPa and +175 MPa. Threshold curves were developed for four different stress ratios, and a clear variation of the threshold stress intensity factor (ΔK_{th}) was identified. The results can be used to understand the vulnerability of fatigue threshold limits and propagation rates based on the surface roughness and residual stress states, thereby to predict and minimise the in-vivo failures of components made of Ti-6Al-4V implant grade material.

Keywords: Fatigue threshold, Residual stress, Stress ratio, Surface roughness, Ti-6Al,4V

1. Introduction

Use of Ti-6Al-4V in industry grew rapidly in Europe and North America in the 1970s [1] because of its excellent biocompatibility, low modulus of elasticity, low stiffness, good tensile properties and high fatigue strength. Currently, manufacture of surgical prostheses has become one of the largest applications of the wrought Ti-6Al-4V with aerospace, nuclear and automotive applications. Titanium forms a bio-inert natural titanium oxide on the surface which resists corrosion, and it possesses low rates of metal iron release, resulting little tendency to cause adverse cell or tissue reactions [2]. Ti-6Al-4V possesses good fatigue strength due to a fine equiaxed microstructure consisting of α and β grains [3]. However, under in-vivo service conditions, the components made of Ti-6Al-4V fail mainly due to randomly varying fluctuating loads. Therefore, design and manufacture of such components to avoid fatigue failure is an important requirement.

Under this study, threshold curves were developed for Ti-6Al-4V, for specific conditions, to understand the variation of safe region under cyclic loads. The stress amplitude ($\Delta\sigma_{th}$) for MSC region and the threshold stress intensity factor range (ΔK_{th}) for different conditions were evaluated. An empirical relationship for the stress intensity factor range based on the notion of an effective crack length $a + a_o$ (a - crack length, a_o-intrinsic material length parameter) was developed for the implant grade of Ti-6Al-4V. The results provide insight into the sensitivity of fatigue threshold limits and crack propagation rates to surface roughness and residual stress states, enabling improved prediction and mitigation of in vivo failures in components manufactured from Ti-6Al-4V implant-grade material. The proposed approach can be used to evaluate the threshold limits (i.e., fatigue-safe envelop) of any material with known surface roughness (defect size) and residual stress state.

1.1 Mean Stress Effect on Fatigue Performance

The stress amplitude (σ_a), mean stress (σ_m), stress ratio (R), and stress range ($\Delta\sigma$) can be defined as,

$$\sigma_a = (\sigma_{max} - \sigma_{min})/2$$

$$\sigma_m = (\sigma_{max} + \sigma_{min})/2$$

$$R = \frac{\sigma_{min}}{\sigma_{max}}$$

$$\Delta\sigma = \sigma_{max} - \sigma_{min}$$

*Eng. (Dr.) **Ruminda J. Wimalasiri**, AMIE(SL), BTech(Hons)(Eng)(OUSL), PhD (SHU, UK), Senior Lecturer, Department of Mechanical Engineering, The Open University of Sri Lanka.*
Email: rjwin@ou.ac.lk
https://orcid.org/0000-0001-8368-5639

Rotary-Bending (R–B) fatigue tests are typically conducted under fully reversed loading conditions ($R = -1$, $\sigma_m = 0$); however, this assumption may be invalid if the test specimens contain residual stresses. One obvious way of accounting for the influence of residual stress on fatigue behaviour is to consider the residual stress value as the local mean stress value [4][5]. Mean stress effects on fatigue can be represented in terms of a constant life diagram. There are different models to correlate the fatigue or endurance limit (S_e) in stress amplitude axis (y-axis), and ultimate tensile strength (S_u), yield strength (S_y) and fracture strength (σ_f) on mean stress axis (X-axis), to provide constant fatigue life. The most well-known models are illustrated in Figure 1 [6].

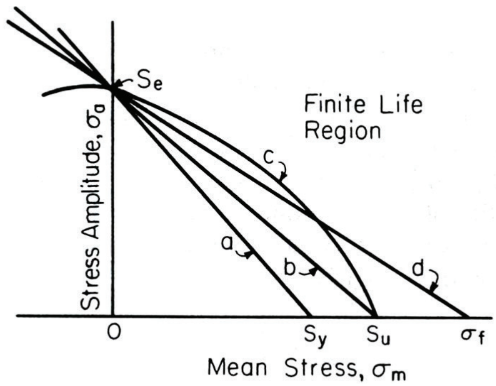

Figure 1 - Comparison of mean stress equations, a. Soderberg, b. Goodman, c. Gerber and d. Morrow

Goodman's criterion has been used for calculations of stress amplitude (σ_a), which is,

$$\frac{\sigma_a}{S_e} + \frac{\sigma_m}{S_u} = 1 \qquad \ldots(1)$$

1.2 Kitagawa-Takahashi (K-T) Type Diagrams

Observing and understanding the behaviour of short fatigue cracks whose size corresponds to that of the microstructural dimension of materials has enhanced the understanding of the fatigue limit phenomena. Before short fatigue crack growth studies, it was believed that below the fatigue/endurance limit cracks would not initiate. However, current knowledge shows that very small cracks may exist, but they may not propagate beyond microstructural barriers that are inherent with the material. Therefore, microstructural characteristics, such as grain size and phase distribution, which result from chemical and mechanical processing and heat treatment, would affect fatigue life and the endurance limit [7].

The most common and traditional way of investigating fatigue behaviour of materials is the S-N or total life approach [8]. In the S-N approach, specimens are subjected to cyclic loading at various stress amplitudes (S) to determine the number of cycles to failure (N). To develop S-N curve by push-pull or R-B fatigue tests, the standard is to have a fully reversed loading. Fatigue crack propagation can be characterized by fracture mechanics-based damage tolerant approach where crack growth rate per cycle (da/dN) studied against the linier elastic stress intensity range ($\Delta K = K_{max} - K_{min}$) during the loading cycle. Using this method, the total number of cycles required to grow a pre-existing flaw to a size required to cause final fracture can be predicted.

The propagation of microscopic defects under dynamic loading can be analysed using K-T type diagram [6], as illustrated in Figure 2. The upper margin of stress for the growth of microscopically short defects (crack size < a_1) is given by the smooth specimen fatigue limit ($\Delta\sigma_e$). The limit of stress for non-propagating long cracks ($a > a_2$) is given by the ΔK_{th}. When the crack length $a > a_2$, Linear Elastic Fracture Mechanics (LEFM) conditions apply and when $a_1 < a < a_2$ the Elastic Plastic Fracture Mechanics (EPFM) conditions apply. Although it is considered that the K-T type diagram is a material property, it is believed that the plot will change due to manufacturing parameters such as residual stress.

Every engineering component has the possibility of containing surface cracks or defects [10]. Even the most carefully prepared engineering surfaces can have micro defects/notches to a depth of 2-3 μm [11], due to manufacturing practices such as, machining, grinding, polishing. Microscopically small cracks behave differently from large cracks. It was also shown that microcracks grow faster than predicted by LEFM calculations in pure titanium and Ti-6Al-4V alloy [12,13,14]. LEFM analysis can be used to calculate the stress-strain fields of engineering components containing defects, but as the size of the initial defect becomes smaller, high stresses needed to propagate the crack. Cracks can propagate below LEFM threshold lengths particularly at high stress levels [11]. According to the K-T method, ΔK_{th} can be expressed in terms of stress range and crack size.

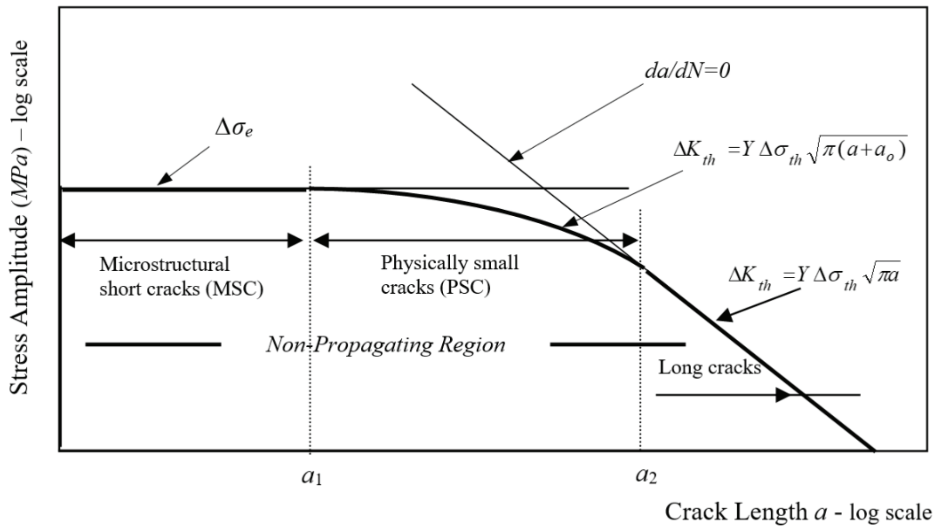

Figure 2 - Schematic representation of K-T type diagram

The LEFM threshold line distinguishes the propagation and non-propagation regions of long cracks, and is given by equation (2),

$$\Delta K_{th} = Y \Delta\sigma_{th}\sqrt{\pi a} \qquad \ldots(2)$$

where, Y is the geometry factor. The equation (2) can be rearranged as follows:

$$log\,\Delta\,\sigma_{th} = -\frac{1}{2} log\,a + log\left(\frac{\Delta K_{th}}{Y\sqrt{\pi}}\right) \qquad \ldots(3)$$

The fatigue limit of a smooth specimen, $\Delta\sigma_e$ (equivalent to $\Delta\sigma_{th}$ for microscopically short defects with crack size < a_1), can be determined experimentally through fatigue testing.

Further to the LEFM concept for a small crack size, El Haddad et. al. [15,16] proposed an empirical relationship for the stress intensity factor range based on the notion of ($a + a_o$). This covers both small and large crack limiting ranges.

$$\Delta K_{th} = Y \Delta\sigma_{th}\sqrt{\pi(a + a_o)} \qquad \ldots(4)$$

The a_o value can be evaluated from the limiting condition where the physical crack size 'a', approaches zero, i.e. $a_o >> a$ and $\Delta\sigma_{th} = \Delta\sigma_e$ [17].

$$a_o = \left(\frac{1}{\pi}\right)\left(\frac{\Delta K}{Y\sigma_e}\right)^2 \qquad \ldots(5)$$

A model was derived to quantify the fatigue limit for a given surface roughness/defect size and surface residual stress state. Equation (5) can be used to calculate the fatigue limit of a component with known surface roughness/defect size and residual stress state. K-T type diagrams were developed to evaluate the safe fatigue envelop.

2. Methodology

2.1 Fatigue Tests

Fatigue tests were performed using a R-B fatigue test machine, which runs at 22 Hz and accommodates a maximum static load of 1200 N. Hour-glass shaped fatigue test specimens were used, with a minimum diameter (d) of 8 mm and a continuous fillet radius of 110 mm. The sample is clamped between two coaxial shafts and subjected to a dead weight while bearings permit rotation. The stress amplitude readings obtained from the R-B machine were validated against calculated values derived from experimentally measured strain using a strain-gauged fatigue specimen. Tests were conducted adhering to ASTM- F 1160-91 [18] and ASTM-F 1659-95 [19] standards. 52 R-B fatigue test samples were used. Samples of four different surface roughness (SR) were prepared, and in each roughness category two subsets were prepared, one annealed (A) and another without annealing (WA) conditions. Figure 3 illustrates the test schedule.

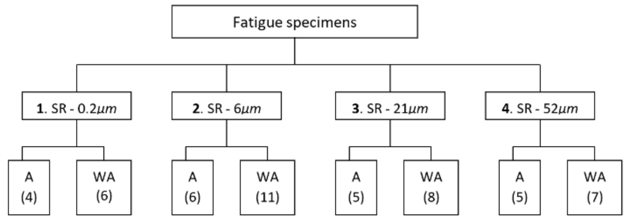

Figure 3 - Test program. Number of samples tested under each set is given within brackets

2.2 Sample Preparation

All samples were initially machined and randomly separated to four batches. These four batches were prepared to 0.2 μm, 6 μm (as machined samples), 21 μm and 52 μm surface roughness (SR). The $R_{z(max)}$, maximum peak to valley height, is considered as the SR value. Samples were prepared to 0.2 μm surface finish (mirror finish) through polishing. Starting with grade 25 μm diamond compound and then 14 μm, 6 μm, 1 μm and finally 0.25 μm diamond compounds were used. The polishing was performed in longitudinal direction. Surface preparation for 21 μm and 52 μm were obtained by roughening the surfaces by No. P60 and P80 silicon carbide grinding papers, respectively. All samples were cleaned thoroughly using industrial methylated spirit. Annealing was carried out under vacuum conditions with a maximum temperature of 700°C for 2 hrs followed by furnace cooling [20].

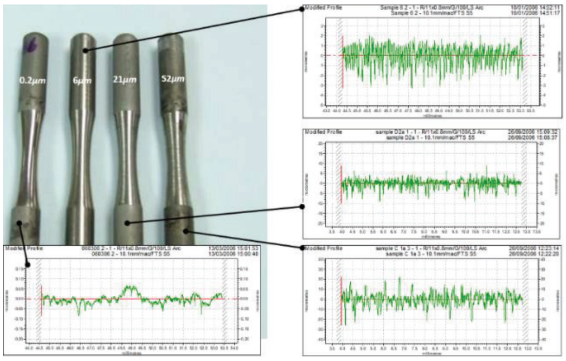

Figure 4 - Surface profiles of four different surface conditions

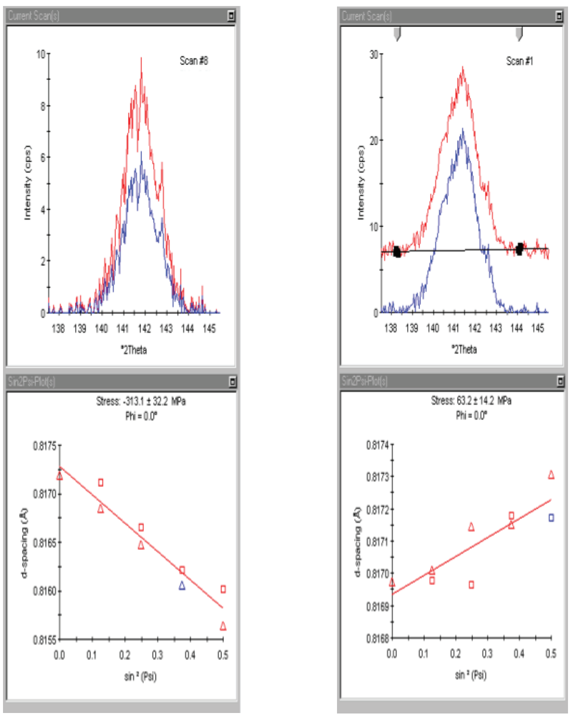

(a) 0.2 μm sample (WA) (b) 0.2 μm sample (A)

Figure 5 - Residual stress measurements of 0.2 μm samples

Surface roughness and residual stress measurements were made prior to fatigue tests. Four surface roughness profiles obtained from Taylor-Hobson Talysurf-120L stylus type apparatus are shown in Figure 4. Residual stress is measured using Philips PW3040 X'Pert Pro XRD, at least two samples from each batch. The results obtained for the two samples are shown in Figure 5.

2.3 Residual Stress Effect to Fatigue Performance

In R-B fatigue tests, it is assumed that the sample undergoes a load cycle of $\sigma_m = 0$ with R = -1. However, in the presence of residual stresses, the mean stress is no longer zero ($\sigma_m \neq 0$) and corresponds to the magnitude of the residual stress; consequently, the stress ratio deviates from −1 ($R \neq -1$).

Consider a R-B test running at stress amplitude of σ_a, and the surface residual stress of the test sample is RS, the schematic diagram of actual load cycle is as shown in Figure 6.

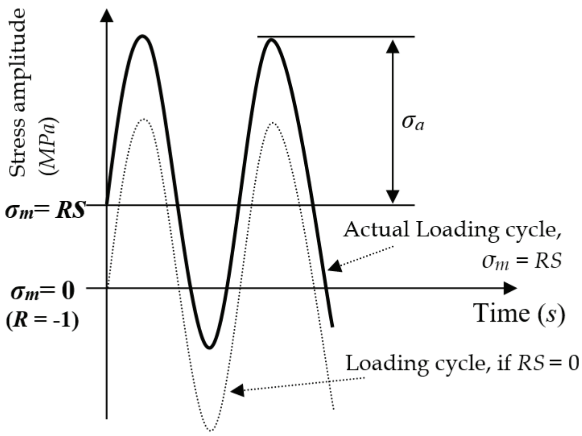

Figure 6 - Variation of mean stress with residual stress

Goodman's criteria given in equation (1) can be used to determine the stress amplitude at the fatigue limit (σ_a) for R = -1. R can be defined as follows.

$$R = \frac{\sigma_{min}}{\sigma_{max}} = \frac{\sigma_m - \sigma_a}{\sigma_m + \sigma_a} \quad \ldots(6)$$

From equations (1) and (6), σ_a in terms of R can be derived as,

$$\sigma_a = \frac{S_u S_e (1-R)}{S_e(1+R) + S_u(1-R)} \quad \ldots(7)$$

Using equation (7), the stress amplitude at particular fatigue limit can be found for any given R. If the stress amplitude ($\sigma_a^{/}$) at the fatigue limit is known for samples having a certain RS, the stress amplitude at fatigue limit for any R can be derived using equations (1) and (7) as,

$$\sigma_a = \frac{\sigma'_a \, S_u \, (1-R)}{\sigma'_a (1+R) + (S_u - R_s)(1-R)} \qquad \ldots(8)$$

At any instance if the RS is known and the stress amplitude at the fatigue limit at that instance (σ_a') is known, the stress amplitude (fatigue limit) for any given R value can be calculated using equation (8).

3. Results and Discussion

3.1 Fatigue Test Results

Fatigue tests were conducted and S-N diagrams obtained at each stage. Figure 7 shows the variation of fatigue endurance limit of WA samples.

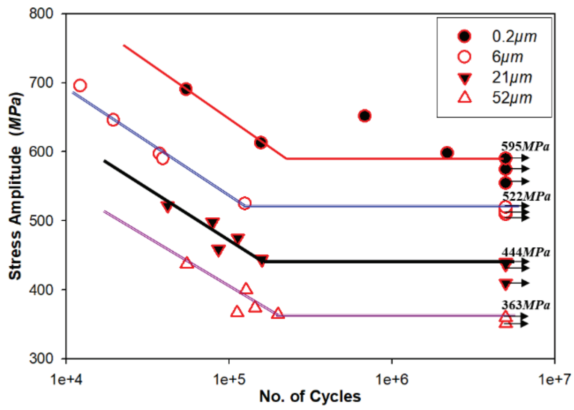

Figure 7 - Variation of fatigue endurance limits of samples WA condition

The variation of fatigue limit for different SR values of 0.2 μm, 6 μm, 21 μm and 52 μm are shown in Figure 8, Figure 9, Figure 10 and Figure 11, respectively, for both A and WA conditions. Respective values of RS and fatigue limit are noted.

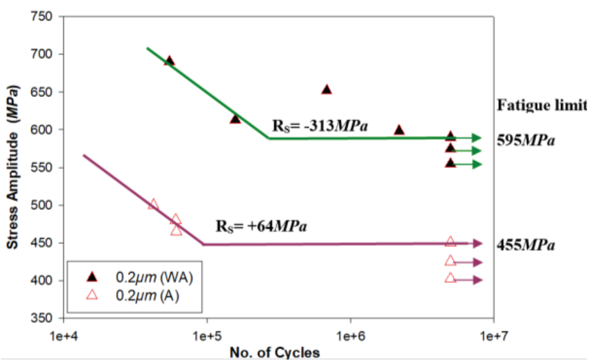

Figure 8 - Fatigue curves of samples finished to a surface roughness of 0.2 μm

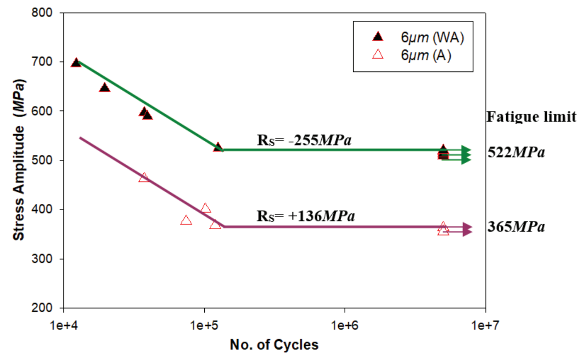

Figure 9 - Fatigue curves of 6μm samples

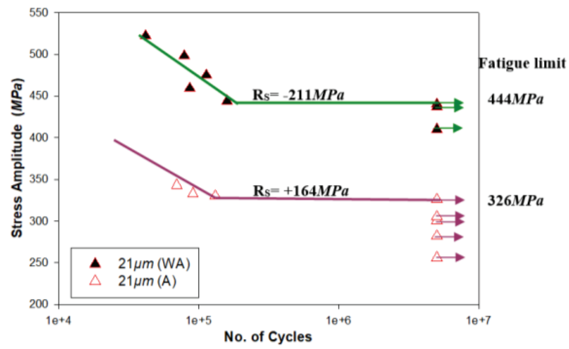

Figure 10 - Fatigue curves of 21 μm samples

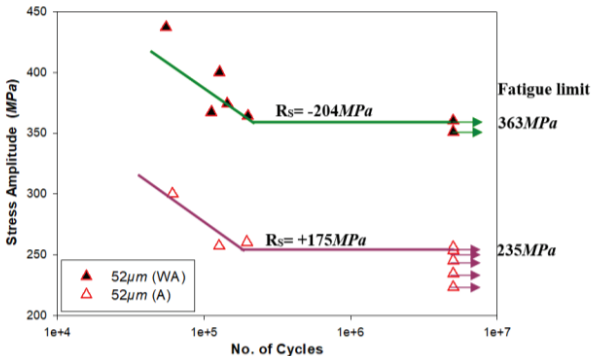

Figure 11 - Fatigue curves of 52 μm samples

A summary of the variation of fatigue limit as a function of surface roughness, for both A an WA conditions, is shown in Table 1.

Table 1 - Fatigue endurance limits. Residual stress values in square brackets

Surface roughness (μm)	**Fatigue limit** MPa **Residual Stress** [MPa]	
	Samples without annealed	**Annealed samples**
0.2	595 [-313]	455 [+64]
6	522 [-255]	365 [+136]
21	444 [-211]	326 [+164]
52	363 [-204]	235 [+175]

A clear variation in residual stress states is observed with changes in surface roughness, highlighting the critical influence of surface finishing processes on the performance of the final product. This effect is particularly significant in fatigue behaviour, where the presence of embedded tensile residual stresses facilitates crack initiation. The variation of fatigue limit vs. residual stress and the surface roughness is illustrated in Figure 12. Before annealing (WA) the residual stresses of the samples are compressive and after annealing stresses become tensile, which will significantly influence the possibility of fatigue initiation and subsequent propagation.

Figure 12 shows the variation of fatigue limit (square brackets) after annealing at each surface roughness condition. This variation is purely due to residual stress since annealing only changes the residual stresses without changing the surface roughness.

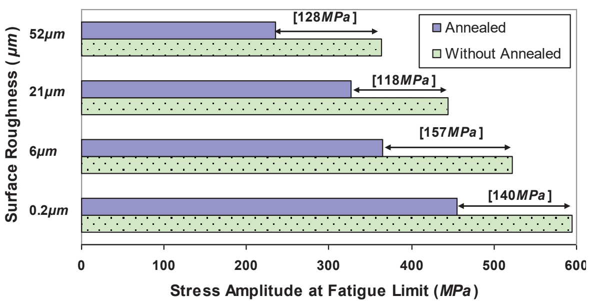

Figure 12 - Variation of fatigue limit due to the change of surface residual stress

3.2 Mean Stress (Residual Stress) Effect to Fatigue Performance of Ti-6Al-4V

The fatigue limit at R = -1 (eliminating the effect of residual stress) is calculated using equation (7), and the results are illustrated in Figure 13.

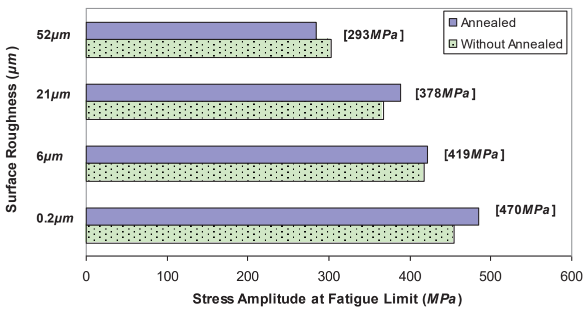

Figure 13 - Calculated fatigue limits for R = -1

The main reason for this analysis is to understand the effect of surface roughness on the fatigue performance. Since the fatigue values are calculated at R = -1, the variation of the fatigue limits solely represents the effect of surface defect size. Actually, in this case, the fatigue limits for both A and WA conditions should be same, but there is a slight change, may be due to experimental errors and measurement errors. So, average value is calculated.

3.3 Effect of Stress Ratio to Fatigue Performance of Ti-6Al-4V

The fatigue limits for positive stress ratio (at R = 0.1) has also been calculated for comparison purposes using equation (8) and are illustrated in Figure 14 for both annealed and non-annealed conditions. Average fatigue limits of both WA and A conditions at each roughness level are noted within square brackets.

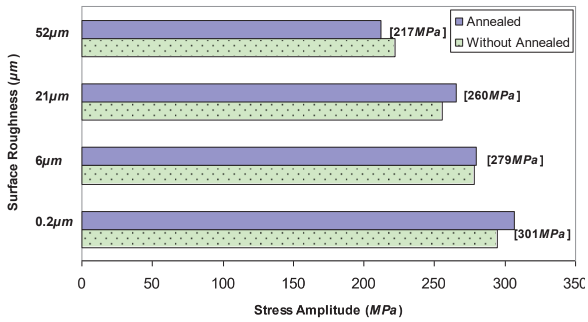

Figure 14 - Calculated fatigue limits for R = 0.1

3.4 Representation of Results in the Form of K-T Type Diagrams

Based on S-N data obtained from experiments, the K-T type diagrams are developed using equations (2) and (4). These diagrams define the variation of the stress amplitude to cause fatigue failure as a function of crack size. The safe region is sensitive to working stress ratio. The value of the ΔK_{th} can be calculated by applying a linear regression analysis to a plot of a vs. $\Delta\sigma_{th}^{-2}$, using equation (4). The value of the geometrical factor, Y, is approximated as unity [21,22,23]. Values of Y for specific crack configurations and loading conditions can be found in literature [24,25].

The K-T type diagrams for WA and A conditions are shown in Figure 15. The ΔK_{th} for the WA and A conditions is $5.9\ \mathrm{MPa}\sqrt{\mathrm{m}}$ and $3.55\ \mathrm{MPa}\sqrt{\mathrm{m}}$, respectively. This compares favourably with literature values of 5 – $6\ \mathrm{MPa}\sqrt{\mathrm{m}}$ [26]. When the crack length reaches around 100 μm, the propagation behaviour approaches that of long cracks. The reduction of the safe working envelope of annealed samples is due to the change of surface residual stress. The threshold stress amplitude for microstructural short cracks reduces from 595 MPa to 455 MPa due to annealing. The importance of residual stress state in fatigue performance, in particular the positive impact from compressive residual stresses can be observed.

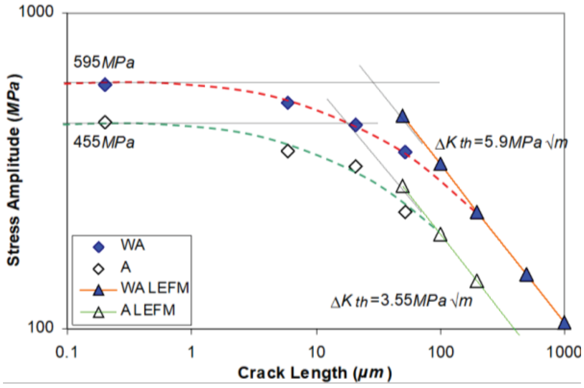

Figure 15 - K-T type diagram showing the estimated threshold stresses for WA and A conditions

The variations of the K-T type diagrams for components with compressive residual stress (WA condition), zero residual stress (R = -1 condition) and tensile residual stress (A condition) are illustrated in Figure 16. The value of a_o is calculated at R = -1 using equation (5), as 33.1 μm.

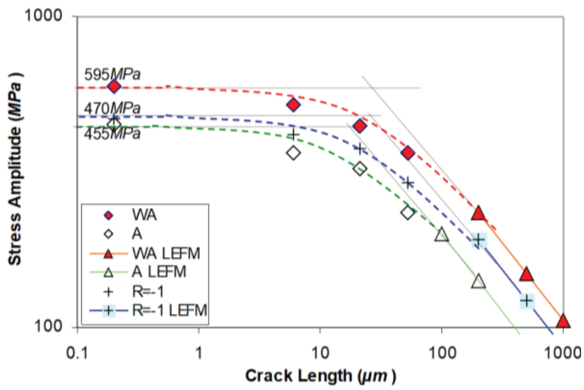

Figure 16 - K-T type diagrams at WA, A and at R = -1 conditions

The comparison of K-T type diagrams for R = -1 and R = 0.1 is shown in Figure 17. A clear reduction of smooth specimen threshold stress amplitude (MSC) and the safe working stress amplitudes for different crack lengths can be observed. The ΔK_{th} can be calculated as 4.8 MPa$\sqrt{m}$ for R = -1 condition and 4 MPa$\sqrt{m}$ for R = 0.1 conditions. Other researchers [16,27,28] show the ΔK_{th} value at R = 0.1 is around 4 MPa$\sqrt{m}$, which shows good agreement between the experiments and the literature. For known flaw sizes, these diagrams facilitate quantitative evaluations of the risk of premature fatigue failures of the components.

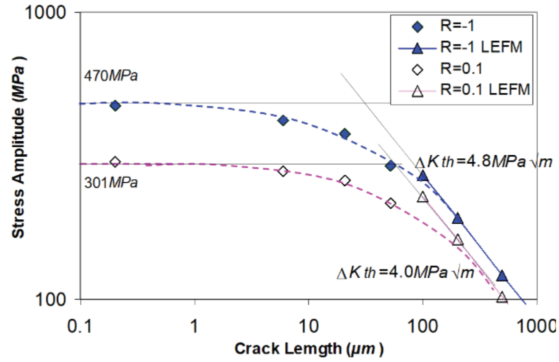

Figure 17 - K-T type diagrams at R = -1 and at R = 0.1 conditions

4. Conclusions

Compressive residual stress enhances the fatigue performance while tensile stress reduces the fatigue performance. Tensile residual stresses and rougher surface finish contract the safe region of K-T type diagrams, while compressive residual stresses and smooth surface finish expand the safe region. Mean stress and stress ratio strongly affect the fatigue performance. The fatigue limit decreases with increasing stress ratio. Reduction of threshold conditions for short cracks (EPFM) and long cracks (LEFM) with the increment of stress ratio can be visualized in K-T type diagrams.

The $\Delta\sigma_{th}$ for MSC region and the ΔK_{th} for different conditions are as follows:

At WA condition:
$\Delta\sigma_{th}$ = 595 MPa, ΔK_{th} = 5.9 MPa$\sqrt{m}$

At A condition:
$\Delta\sigma_{th}$ = 455 MPa, ΔK_{th} = 3.6 MPa$\sqrt{m}$

For R = -1:
$\Delta\sigma_{th}$ = 470 MPa, ΔK_{th} = 4.8 MPa$\sqrt{m}$

For R = 0.1:
$\Delta\sigma_{th}$ = 301 MPa, ΔK_{th} = 4.0 MPa$\sqrt{m}$

For fully reversed loading, the value of a_o is calculated as 33.1 μm. So, the equation (4) can be specified to the grade of Ti-6Al-4V examined under this study as,

$$\Delta K_{th} = Y\Delta\sigma_{th}\sqrt{\pi(a+33.1)}$$

This approach can be used to evaluate the threshold limits (i.e. fatigue safe envelop) of any material with known surface roughness/defect size and residual stress state.

Acknowledgement

Author wishes to acknowledge the immense guidance given by Dr. Upul S. Fernando, Prof. Robert Akid, and Dr. Anita Clark.

References

1. Brunette, D. M., Tengvall, P., Textor, M., Thomson, P., Titanium in Medicine, Sringer, Springer-Verlag Berlin Heidelberg, 2001; ISBN 3-540-66936-1.
2. Machado, A.R., Wallbank, J., Machining of titanium and its alloys- a review, *Proc Inst Mech* Engrs, 1989; Vol. 204, p. 53-60.
3. Sitting, C., Textor, N., Spencer, N. D., Surface characterization of implant materials c.p. Ti, Ti-6Al-7Nb and Ti-6Al-4V with different pretreatments, *Journal of Materials in Medicine*, 1999, 10, p 35-46.
4. Handbook of Residual Stress and Deformation of Steel, ASM International, ISBN 0-87170-729-2, March 2005.
5. Hines, J. A., Peters, J. O., Lutjering, G. L., Microcrack Propagation in Ti-6Al-4V Alloys, Fatigue Behaviour of Titanium Alloys, 1999.
6. Kitagawa, H., Takahashi, S., Applicability of fracture mechanics to very small cracks or the cracks in the early stage, *In: Proceedings of the Second International Conference on Mechanical Behaviour of Materials*. Metals Park, OH: ASM; 1976; p. 627–31.
7. Bannatine, J. A., Comer, J. J., Handrock, J. L., Fundamentals of Metal Fatigue Analysis, Prentice Hall, Englewood Cliffs, New Jersey 07632, ISBN 0-13-340191-X.
8. Akid, R., Miller, K. J., Short fatigue crack behaviour of low carbon steel under corrosion fatigue condition, *Fatigue FractEngng Mater Struct*, 1991; vol14, no 6, p. 637-49.
9. Wohler, A., (1860) Versuche uber die festigkeit dev eisenbahnwagenachsen, Seitschrift fur Bauwesen 10; English Summary (1867), *Engineering*, 4,160-1.
10. The behaviour of short fatigue cracks, edited by Miller K. J., de los Rios E. R., Mechanical Engineering Publications Ltd, London, 1986, pp 2.
11. Vasudevan, A. K., Sadananda, K., Glinka, G., Critical parameters for fatigue damage, *International Journal of Fatigue*, Volume 23, Supplement 1, 2001, Pages 39-53.
12. Wnager, L., Lutjering, G., Microstructural Influence on Propagation Behaviour of Short Cracks in an (α+β) Ti Alloy, *Zeitschrift fur metallkunde*, 1987; 78, 5, p. 369-75.
13. Pearson, S., Initiation of fatigue cracks in commercial aluminium alloys and the subsequent propagation of very short cracks, *EngngFract Mech*, 1975; 7, p. 135-47.
14. Hines, J. A., Lutjering, G., Propagation of microcracks at stress amplitudes below the conventional fatigue limit for three references, *Fatigue FractEngng Mater Struct*, 1999; vol.22, iss.8, p. 657-65.
15. El Haddad, M. H., Smith, K. N., Topper, T. H., Fatigue crack propagation of short cracks, *American Society of Mechanical Engineering,* Revised manuscript, Feb 15, 1978; Paper No. 78-mat-7.
16. El Haddad, M. H., Topper, T. H., Topper, T. N., Fatigue life prediction of a smooth and notched specimens based on the fracture mechanics, *Journal of Engineering Materials and Technology*, 1980; p. 91- 96.
17. Chapetti, M. D., Application of a threshold curve model to high cycle fatigue behaviour of small cracks induced by foreign-object damage in Ti-6Al-4V, *International Journal of Fatigue*, 2005; 27, p. 493-501.
18. Turnbull, Z. S., Influence of pitting on the fatigue life of a turbine blade steel, Blackwell Science Ltd. *Fatigue FractEngng Mater Struct*, 1999; 22, p. 1083-93.
19. ASTM F 1160-91; 'Standard Test Method for Constant Stress Amplitude Fatigue Testing of Porous Metal-Coated Metallic Materials'.
20. ASTM F 1659-95; 'Standard Test Method for Bending and Shear Fatigue Testing of Calcium Phosphate Coatings on Solid Metallic Substrates'.
21. Bolton, W., Newnes Engineering Materials Pocket Book, Third Edition, Newnes, ISBN 0-7506-4974-7.
22. Kruzic, J. J., Ritchie, R. O., Technical note; Kitagawa-Takahashi diagrams define the limiting conditions for cyclic fatigue in human dentin, Published online 29 September 2006 in Wiley InterScience (www.interscience.wiley.com). DOI: 10.1002/jbm.a.30939.
23. Hudak, S. J. Jr., Small crack behaviour and the prediction of fatigue life, Transaction of the *ASME*, 26, Vol.103, January 1981.
24. Moshier, M. A., Nicholas, T., Hillberry, B. M., High cycle fatigue threshold in the presence of naturally initiated small surface cracks, ASTM special publications, 2002, 1417, 129-146.
25. Murakami, Y., editor. Stress Intensity Factors Handbook, 1st ed. Elmsford, NY: Pergamon; 1987. Vol. 1, 640 pp.
26. Tada, H., Paris, P. C., Irwin, G. R., The Stress Analysis of Cracks Handbook. New York: ASME Press; 2000. 677 pp.
27. Brown, C. W., Smith, G. C., The Effect of Microstructure and Texture on the fatigue Crack Growth Threshold in Ti-6Al-4V, *Intergovernmental Conference-EU*, 1982, Vol 1, 329-343.
28. Boyer, R., Welsch, G., Collongs E. W., Materials Properties Handbook: Titanium Alloys, ASM International, 1994; ISBN 0-87170-481-1.
29. Sadanandan, K., Vasudevan, A. K., Fatigue crack growth behaviour of titanium alloys, *International Journal of Fatigue*,2005;27, p.1255-66.